IOPscience iopscience.iop.org

Home Search Collections Journals About Contact us My IOPscience

Electron Emission Properties of Nitrogen-Induced Localized Defects in InAsN/GaAs Quantum Dots

This content has been downloaded from IOPscience. Please scroll down to see the full text.

2011 Jpn. J. Appl. Phys. 50 111001

(http://iopscience.iop.org/1347-4065/50/11R/111001)

View the table of contents for this issue, or go to the journal homepage for more

Download details:

IP Address: 140.113.38.11
This content was downloaded on 28/04/2014 at 22:55

Please note that terms and conditions apply.

Japanese Journal of Applied Physics **50** (2011) 111001 **REGULAR PAPER**
DOI: 10.1143/JJAP.50.111001

Electron Emission Properties of Nitrogen-Induced Localized Defects in InAsN/GaAs Quantum Dots

Cheng-Hong Yang[1]*, Meng-Chien Hsieh[1], Chia-Wei Wu[1], Yen-Ting Chang[1],
Yue-Han Wu[2], Li Chang[2], and Jenn-Fang Chen[1]

[1] *Department of Electrophysics National Chiao Tung University, Hsinchu 30010, Taiwan, R.O.C.*
[2] *Department of Materials Science and Engineering National Chiao Tung University, Hsinchu 30010, Taiwan, R.O.C.*

Received March 31, 2011; accepted July 26, 2011; published online October 25, 2011

The electron-emission properties of nitrogen-induced (N-induced) localized defects in InAsN/GaAs quantum dots (QDs) are investigated in detail by capacitance–voltage (*C*–*V*) profiling and bias-dependent deep-level transient spectroscopy (DLTS). The incorporation of nitrogen (N) into InAs QDs is shown to produce localized defects near QDs and threading-dislocation-related defects in the top GaAs layer. The threading dislocation is associated with an electron-emission energy of approximately 0.648 eV and emission from the sample surface toward the QDs. The electron-emission energy from the QDs associated with the localized defects increases from 0.19 to 0.36 eV, indicating that both types of defect near QDs have low electron emission energies. Therefore, the change in emission energy is attributable to the defects across the QD interface where a band offset exists. The *C*–*V* profile at 300 K shows extended carrier depletion near the QDs. As ac frequency increases, an electron-emission peak emerges at the QDs; this peak is followed by another prominent peak, suggesting that the localized defect that is responsible for this latter peak has an energy below the QD electron ground state. On the basis of a *C*–*V* profile simulation, this defect is located at the QD at the observed emission energy below the GaAs conduction band, 360 meV. A comparison with InAsN QD and strain relaxation InAs QD samples reveals that the localized defect arises from a nitrogen alloy fluctuation in the QD. The energy location of this defect reveals a possibility that incorporated N is associated with a particular mode. © 2011 The Japan Society of Applied Physics

1. Introduction

InAsN/GaAs self-assembled quantum dots (QDs) have recently attracted considerable attention[1–4] because of their potential use in the realization of long-wavelength optoelectronic devices. Lasers that are made of this material and emit at 1.3 or 1.55 µm have been demonstrated.[2–6] However, the incorporation of nitrogen (N) considerably reduces photoluminescence (PL) efficiency owing to the N composition fluctuation effect.[5,7] The effects of composition fluctuation in this material system have been studied by PL measurement, transmission electron microscopy (TEM), and deep-level transient spectroscopy (DLTS).[8–12] Despite these efforts, little is known about the details of the relationship between N content and electrical properties. Furthermore, although the optical states that are induced by composition fluctuation have been investigated,[13] to the best of the authors' knowledge, electrical states that are induced by composition fluctuation have seldom been investigated. However, many researchers who have sought to elucidate electrical states have focused on experimentally determining the electronic band structure of a QD by analyzing electron emission from the QD. Therefore, in this investigation, we study the properties of the nitrogen-induced (N-induced) trap that is formed by the incorporation of N into InAs QDs. The electrical properties of such an N-induced trap were characterized by frequency-dependent capacitance–voltage (*C*–*V*) and DLTS measurements. However, as the probed sample does not have a simple bulk structure, analysis of DLTS spectra is difficult because the band structure affects the emission parameters (like depletion region), which therefore depend on the applied voltage. This investigation demonstrates an important effect of the electronic band structure. The selection of a small step voltage enables the resolution of the DLTS spectra of N-induced traps. A simple *C*–*V* profile is obtained and the band structure is simulated to obtain important information about the electron-emission parameters of an N-induced trap.

2. Experimental Methods

InAsN QDs were grown on an n+-GaAs(100) substrate by molecular beam epitaxy in a Riber Epineat machine. An InAs QD structure, consisting of a 2.2 monolayer (ML) InAs layer and a 60 Å $In_{0.15}Ga_{0.85}As$ cap layer that was grown at a rate of 1.86 Å/s at 480 °C, was sandwiched between two 300-nm-thick Si-doped GaAs ($\sim 8 \times 10^{16}$ cm^{-3}) barrier layers. Indium and gallium were supplied from Knudsen cells, and arsenic in the form of As_2 was supplied from a cracker source. N atoms were incorporated into the InAs layer from ultra pure N_2 gas using an EPI-Unibulb radio-frequency (RF) plasma source at a N_2 flow rate of 0.15 sccm and an RF power of 250 W. Based on the assumptions that all of the added N was incorporated into the InAs sublattice and that the efficiency of N incorporation was similar to that in the GaAsN layer, the N content must have been much larger than 3%, as determined from the growth rates of the InAs (0.26 Å/s) and GaAs (2.78 Å/s) layers. Such a high N content is associated with the very low growth rate of the InAs QDs layer and is responsible for the high density of QDs. As N atoms are incorporated into the InAs layer, N atoms are obvious on the surface of the InAs QD layer. Post growth rapid thermal annealing was performed. Schottky diodes were realized by evaporating Al with a dot diameter of 1500 µm after the sample surface had been slightly chemically etched. In other respects, the sample of N-free InAs QDs had the same layered structure as it would have without the incorporation of N. A typical InAs QD sheet density of about 1×10^{10} cm^{-2} was observed by atomic force microscopy (AFM). *C*–*V* profiling and admittance spectroscopy were performed using an HP 4194A impedance analyzer. PL measurements were made using a double-frequency Nd-doped yttrium aluminum garnet laser at 532 nm.

*E-mail address: jion@mail2000.com.tw

 © 2011 The Japan Society of Applied Physics

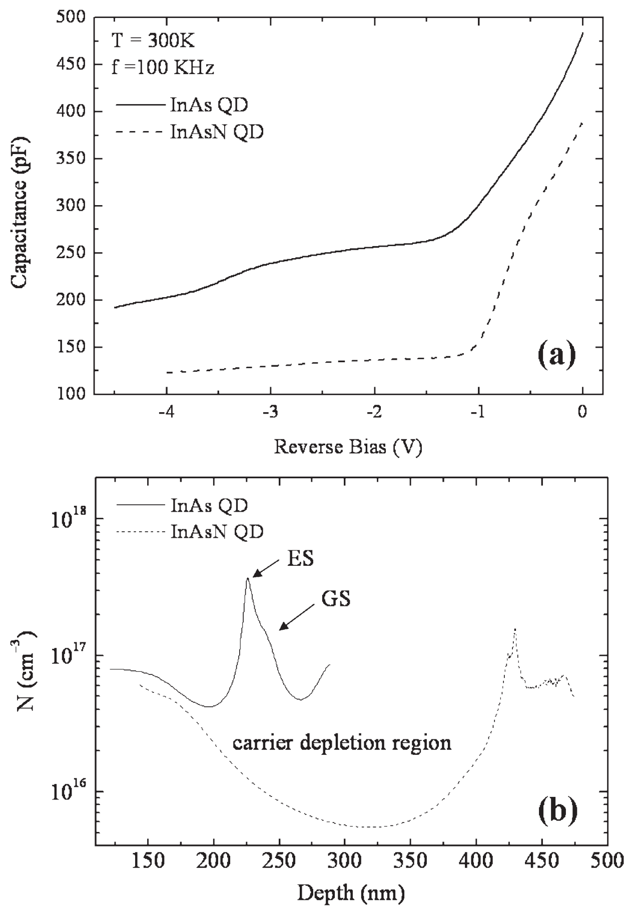

Fig. 1. (a) 300-K *C–V* and (b) concentration profiles measured at 1 M KHz for the normal InAs QD and InAsN QD samples. The concentration profile of the normal InAs QD reveals two carrier accumulations, ES and GS, related to the first excited state and ground state in the InAs QD, respectively. On the other hand, N incorporation into InAs QD produces N-induced traps, and the traps cause carrier depletion near the dot (300 nm) and neighboring GaAs layers.

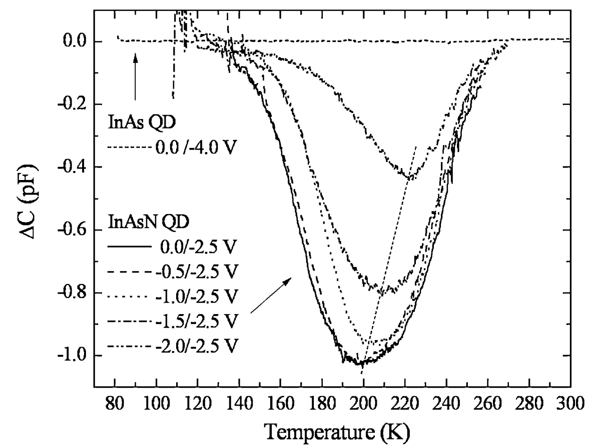

Fig. 2. DLTS spectra of the normal InAs QDs and InAsN QDs, measured at different quiescent voltages with a fixed sweeping step of 0.5 V. In the InAs QDs sample, no signals are observed in the GaAs layer. For a quiescent voltage of −2.0 V (−2.0 to −2.5 V), a trap signal can be seen at approximately 220 K with an activation energy of 293 meV for the InAsN QD sample. On fixing the depletion bias (−2.5 V) and reduced step pulse bias to −0.5 V, the signal of N-induced localized defect is saturated. In addition, as V_P increases to 0 V gradually, the peak has a downward temperature shift, which would reduce electron emission time and activation energy. This result shows that the N-induced localized defect causes an upward energy shift in the QD. These phenomena reveal the finite density of states property of N-induced localized defects.

3. Results and Discussion

3.1 Carrier distribution and DLTS measurement

In previous studies of transmission electron emission,[14] the incorporation of N into InAs QDs has been shown to relax by the induction of threading dislocations in the top GaAs layer and localized defects near the QDs. The threading dislocations that propagate from the QDs to the surface of the sample are probably generated by the gliding of interfacial dislocations, because elastic strain is associated with a shear stress.[15,16] In contrast, a N-induced localized defect ($E_{\rm local}$ defect) does not propagate into the GaAs layers but is confined near QDs, suggesting the presence of N composition fluctuation. Figures 1(a) and 1(b) show the 300-K *C–V* and converted concentration profiles of InAs and InAsN QD samples, respectively, measured at 1 MHz. The InAsN QD sample is relaxed because the localized defect state is similar to the states of those defects observed in strain-relaxed QDs or InGaAs/GaAs quantum wells when the InAs deposition thickness exceeds a critical thickness.[17] The 2.2 ML InAs QD sample exhibits two strong electron accumulations that originate from the electron ground energy state (GS) and the electron first excited state (ES) of the InAs QDs, and the depths of these electron accumulations are smaller than the depth of the QDs (300 nm) because this sample was slightly chemically etched before Schottky metal evaporation. The InAsN QD sample exhibits carrier depletion at the dots (300 nm) and neighboring GaAs layer and induces the formation of electron defects, which depletes the electrons of QDs. DLTS measurements were made to identify the electron defects. Figure 2 shows the obtained spectra of the InAs and InAsN QD samples. The sweeping voltages are as indicated. Whereas the InAs QD sample exhibits no defects, the InAsN QD sample exhibits a broad signal at a low temperature, superimposed upon a background signal, suggesting the presence of significant $E_{\rm local}$ defect. Furthermore, the DLTS spectra of InAsN QDs are obtained at a reverse bias maintained at −2.5 V, which is sufficiently high to enable all electrons in the $E_{\rm local}$ defect to be depleted and step pulse bias is reduced to −0.5 V. The spectra clearly reveal a saturated peak at −0.5/−2.5 V. The rate window is 4.3 ms and the filling pulse time is set to 10 ms to ensure saturation of the height of the peak from the $E_{\rm local}$ defect. The dashed line indicates that the peak temperature of the $E_{\rm local}$ defect shifts as the pulse bias decreased. This strong dependence on bias explains the fact that the last trace represents the maximum filling of the dots, and hence a systematic shift of the peak temperature downward by approximately 6 K is observed as pulse bias is reduced. Figure 3 reveals that when the step voltage is reduced to −0.5 V (superimposed upon a quiescent bias in the range from 0 to −3.5 V), the spectrum can be resolved into two prominent defects ($E_{\rm local}$ defect and $E_{\rm thread}$ defect), namely, $E_{\rm local}$ defect from −1.0/−1.5 V to −3.0/−3.5 V (activation energy from 190 to 360 meV) and $E_{\rm thread}$ defect from −0/−0.5 V to −2.5/−3 V (activation energy from 842 to 648 meV); the rate window is 4.3 ms

© 2011 The Japan Society of Applied Physics

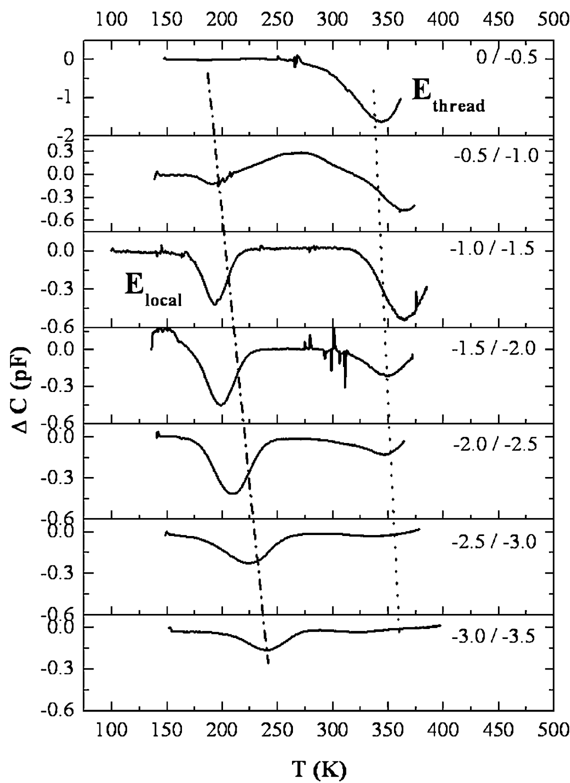

Fig. 3. DLTS spectra of the InAsN QD sample, showing two traps; E_{local} defect is associated with the N-induced localized defects near the QD and E_{thread} defect is associated with the threading dislocations in the top GaAs. With increasing reverse quiescent bias, the peak temperature of the E_{local} defects shifts toward a higher temperature, reflecting the presence of continuous energy states below the GaAs conduction band edge, to which electrons are emitted from the E_{local} defects. On the other hand, the peak temperature of the E_{thread} defects seems to be fixed at 350 K, suggesting the presence of continuous state distribution below the GaAs conduction band edge from 842 to 648 meV. This result can be explained that traps are present across the QD interface where a band offset exists.

Table I. Electron thermal emission energies and capture cross sections of the N-induced localized defect and threading dislocation defect, measured at different quiescent voltages with a fixed sweeping step of 0.5 V for the as-grown sample.

Bias (V)	E_{local} (meV)	Capture cross section (cm^2)	E_{thread} (meV)	Capture cross section (cm^2)
$-0.5/-1.0$	193	9.8×10^{-19}	842	7.6×10^{-17}
$-1.0/-1.5$	199	1.1×10^{-18}	772	2.2×10^{-16}
$-1.5/-2.0$	210	1.4×10^{-18}	768	3.4×10^{-15}
$-2.0/-2.5$	293	2.0×10^{-17}	741	8.8×10^{-15}
$-2.5/-3.0$	320	1.8×10^{-17}	712	3.1×10^{-14}
$-3.0/-3.5$	360	6.3×10^{-17}	648	4.9×10^{-14}

and the filling pulse time is set to 10 ms. Table I shows a summary of the bias-dependent activation energies and capture cross sections of the InAsN QD sample. The DLTS spectra in Figs. 2 and 3 and the C–V curve in Fig. 1(a) are used to determine the concentrations and spatial locations of the E_{local} defect. The effective density of E_{local} defects (N_{local}) is calculated using the equation $N_{local} = N_d \cdot (\Delta C/C_0{}^2) \cdot \varepsilon_{GaAs}\varepsilon_0 A$, and N_{local} is about 4×10^{10} cm^{-2}. Here, the Schottky constant area (A) is 5×10^{-3} cm^2; the saturated peak height (ΔC) is 1 pF; $N_d = 8 \times 10^{16}$ cm^{-3}, and the capacitance (C_0) of the C–V plateau is 105 pF. This density is larger than QD sheet density (about 1×10^{10} cm^2 for InAs QD sheet density measured by AFM). Thus, the concentration of defect states is large enough to deplete all of the electrons in the QDs. This finding explains why both the peak of quantum dot emission (QE) and that of E_{local} defect are obtained. These peaks are consistent with the PL spectra, which clearly show the QD GS and E_{local} defect state at 300 K. The spatial location is simply obtained from the edge of the depletion region of the C–V curve. For E_{local} defect observed at $-0.5/-1.0$ V, the depletion bias of -1.0 V is used to identify the edge of the depletion region. A defect donates carriers only when the Fermi level crosses E_{local} defect. However, at this point, the energy depth of the E_{local} defect causes the edge of the depletion region to be deeper than the crossing point, and thus the obtained location is deeper than the actual location of the defects. In a simple simulation, a trap that is located at the QDs (300 nm) and 360 meV below the GaAs conduction band edge yields a signal at 350 nm. Thus, the location in Fig. 1(b) at which the depth is 350 nm can be roughly treated as the location of the QDs; hence, the E_{local} defect is between the surface of the sample and a depth that is near QDs.

3.2 Properties of the threading dislocation defect

As shown in Fig. 3 and Table I, the electron emission energy of E_{thread} decreases from 842 meV ($\sigma = 7.6 \times 10^{-13}$ cm^{-2}) for $-0.0/-0.5$ V to 648 meV ($\sigma = 5.6 \times 10^{-15}$ cm^{-2}) for $-3.0/-3.5$ V. The DLTS peak height of the E_{thread} defect shows no saturation, even when the filling pulse duration time is increased to 100 ms. This feature is consistent with the capacitance-time transience of the defects associated with the threading dislocation, which exhibits a logarithmic function.[15,16] This defect is believed to be defect EL2 (841 meV) in bulk GaAs, as reported by Irvine *et al.*[18] who investigated InGaAs layers with various In contents, and observed an EL2 defect at 620 meV from 0 to 0.18 in an $In_xGa_{1-x}As$ layer grown on GaAs. The obtained electron emission energy in bulk GaAs was smaller than that in the InGaAs layer grown on GaAs, suggesting that the defect was probably associated with the valence band edge; thus, the difference between emission energies may have been the difference between the band gaps of GaAs and InGaAs. This band structure effect explains the decrease in the emission energy of the E_{thread} defect. The emission energy of a defect typically increases as the band gap of the host material is reduced.

3.3 Electron emission from QDs

As shown in Fig. 1(b), the InAsN QD sample is depleted of electrons. This depletion is presumably caused by the E_{local} defects, which must lie at an energy below the QD electron GS. Since the emission time is long, electrons that are trapped in the E_{local} defects can not follow the alternating current (ac) signal to be modulated. This depletion remains as the frequency is lowered to 3 kHz. However, electron emission from the defects can be activated directly by increasing the frequency to decrease emission time. Figure 4 shows the C–V curve at 300 K and the corresponding depth

 © 2011 The Japan Society of Applied Physics

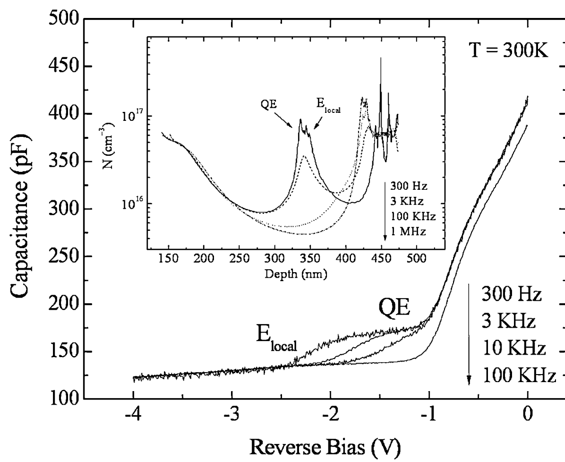

Fig. 4. C–V spectra of the InAsN QD sample and the corresponding concentration profiles in the inset, measured at 300 K. As frequency is reduced to 300 Hz, the C–V spectra show a capacitance plateau, corresponding to an electron-emission peak from the QD, and an other extra capacitance plateau, corresponding to electron-emission from E_{local} defect.

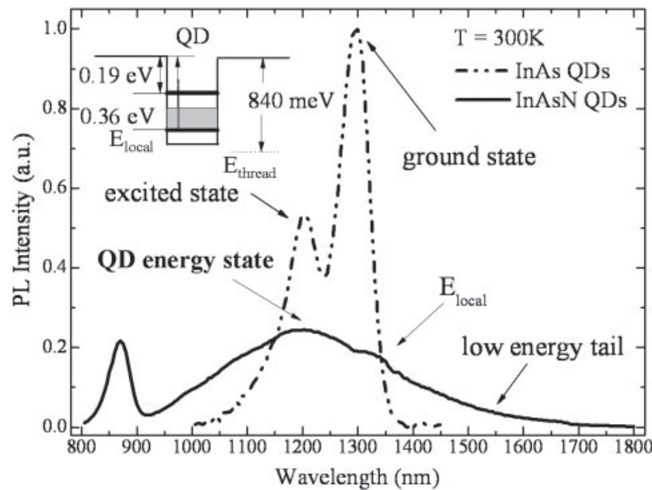

Fig. 5. 300 K PL spectra of normal InAs QD and InAsN QD samples, showing a blue-shift of the QD ground transition. N incorporation into InAs QDs severely degrades QD quality. Also included is a schematic conduction band diagram showing the QD electron ground state (at 0.2 eV below the GaAs conduction band edge) and energy and spatial locations of the threading dislocation defect and N-induced localized defect.

profiles at 300 K in the inset of Fig. 4. The profile shows a similar carrier depletion at 1 MHz; however, at 300 Hz, a capacitance plateau at approximately -1.5 V and another capacitance plateau at approximately -2 V emerge. The capacitance plateau at approximately -1.5 V is converted to a carrier-accumulation peak that is centered at 330 nm. The depth is close to the location of the InAs(N) QD samples at 300 nm; thus, the peak is associated with electron emission from QD electron states and is designated as the QE peak. The presence of the QD electron states is determined from the 300 K PL spectra of the InAs QD and InAsN QD samples, which are shown in Fig. 5. The InAs sample shows QD GS emission at 0.953 eV (1300 nm), which is blue-shifted to 1.03 eV (1200 nm) in the InAsN QD sample, presumably by a strain relaxation, which occurs to reduce dot size.[19,20] The peak of the InAsN QD sample is only slightly broader than that of the InAs QD sample and it is asymmetric with a long low-energy tail that extends to 1500 nm,[21] suggesting that the incorporation of N does not destroy the QD electron GS or cause emission from an extra E_{local} defect at 1330 nm. Kapteyn *et al.*[22] estimated a confinement energy of 0.19 eV for the electron ground state of InAs QDs, which emit at a wavelength that is close to that emitted by the InAsN QDs herein (1.03 eV at 300 K). Thus, the QD GS is 0.19 eV below the GaAs conduction band edge, as shown in the simplified schematic conduction band diagram in Fig. 5. The energy locations of E_{thread} and E_{local} defects are also displayed, neglecting the effect of the band structure. Therefore, the electron GS emission energies are approximately from 0.19 to 0.21 eV and the E_{local} defect emission energy is from 0.29 to 0.36 eV in Table I.

3.4 Depth-profile simulation of the localized defect

The capacitance plateau at -2 V in Fig. 4 may arise from electron emission from the E_{local} defect. From the DLTS spectra, the emission rate of the E_{local} defect (at 360 meV for $-3.0/-3.5$ V) can be extrapolated to 900 Hz at 300 K. This frequency exceeds the ac modulating frequency of 300 Hz, and allows the modulation of the E_{local} defect. This capacitance plateau is seen after the QE peak, suggesting that the E_{local} defect lies below the QD GS, consistent with the carrier-depletion effect. To determine to what energy level the electron-emission energy is related, the C–V profile is simulated by solving the Possion equation for an n-type GaAs Schottky diode (with a barrier height of 0.8 eV) with a back ground doping concentration of 8×10^{16} cm^{-3}, an electron quantum energy state number of 3×10^{16} cm^{-3} at the QD (300 nm) with a thickness of 3 nm (equivalent to a sheet concentration of 1×10^{10} cm^{-2}) and an energy 200 meV below the GaAs conduction band edge, and a defect number of 6×10^{16} cm^{-3} at the QD (300 nm) with a thickness of 3 nm (equivalent to a sheet concentration of 2×10^{10} cm^{-2}) and at 360 meV below the GaAs conduction band edge, as shown in Fig. 6(a). Figure 6(b) shows the simulated C–V profile: the S curve represents the C–V profile of a classical n-type GaAs Schottky diode, the Q curve represents the C–V profile of an n-type GaAs Schottky diode including an electron GS of QD at 200 meV, and the T curve represents the C–V profile of an n-type GaAs Schottky diode including an electron quantum dot energy state at 200 meV and an extra defect at 360 meV. The simulated results generally are broadly consistent with the experimental curves in Fig. 4.

3.5 Comparison with relaxed InAs QDs

The incorporation of N causes a blue-shift to 1200 nm. This blue-shift is associated with the formation of smaller QDs, as revealed in a TEM image in Fig. 7(b) (with a base of 10 nm and a height of 3 nm), and of the normal InAs QDs (without N) as revealed in a TEM image in Fig. 7(a) (with a base of 20 nm and a height of 7 nm). The InAs QD sheet density estimated from the TEM image in Fig. 7(a) is about 1.25×10^{10} cm^{-2}, which corresponds to the InAs QD sheet density estimated from an AFM image of an InAs QD

© 2011 The Japan Society of Applied Physics

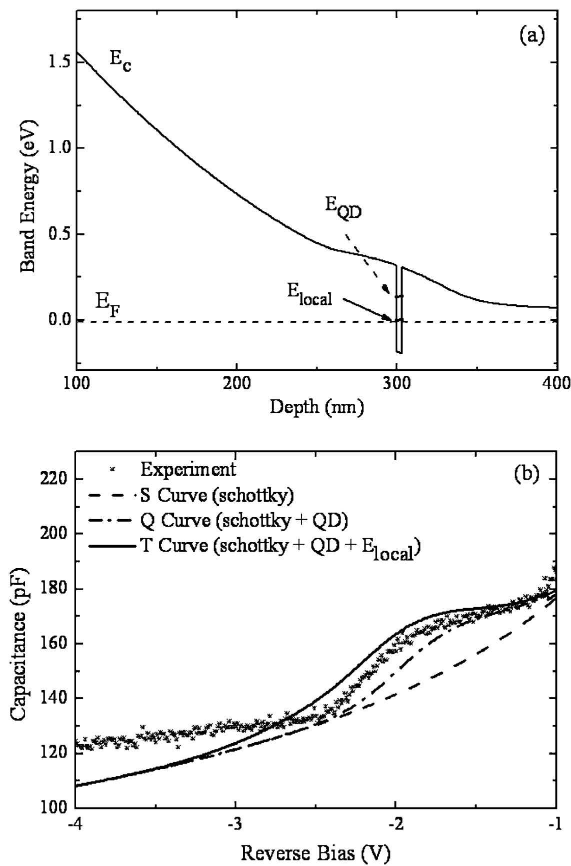

Fig. 6. (a) Energy band diagram used for simulation, assuming the presence of a QD state (0.2 eV below GaAs conduction band) with a concentration of 3×10^{16} cm^{-3} and a defect (0.35 eV below GaAs conduction band) below the QD state with a concentration of 6×10^{16} cm^{-3} with a thickness of 3 nm (3.3 nm in QD layer height). (b) C–V spectra simulated under three conditions depending on ac frequency and dc sweeping rate: the S curve represents a classic energy band of the GaAs Schottky diode, the Q curve represents the trapped electrons in the QD state can follow the ac signal, and the T curve represents the trapped electrons in the QD state and the defect can follow the ac signal.

sample. Similarly, the InAsN QD sheet density is estimated to be about 3.8×10^{10} cm^{-2}, which is more than the InAs QD sheet density and near the N_{local} defects. Hence, this result confirms that the N_{local} defect states originate from the incorporation of N into InAs QDs. This defect is believed to arise from the possibility that the N atom may change the surface potential due to its strong bond, and also decreases the migration length at the surface, as reported by Makino *et al.*[23] Therefore, InAsN QD density increases, and InAsN QD size decreases. In addition, this phenomenon is suspected to be the result of strain relaxation that occurs in the QDs, since lattice misfits are observed near the QDs. Strain relaxation in the InAs QDs was previously shown to cause a sudden blue-shift of 78 meV when the InAs deposition thickness exceeds a critical thickness of 3 ML.[24] This result shows that the incorporation of N causes an upward energy shift of the QD electron state, which would reduce emission time and energy. However, the experimental data reveal an opposite trend, excluding the energy shift of the QD state as a possible cause of the increase in emission time. Hence, the significant increase in emission time and energy can

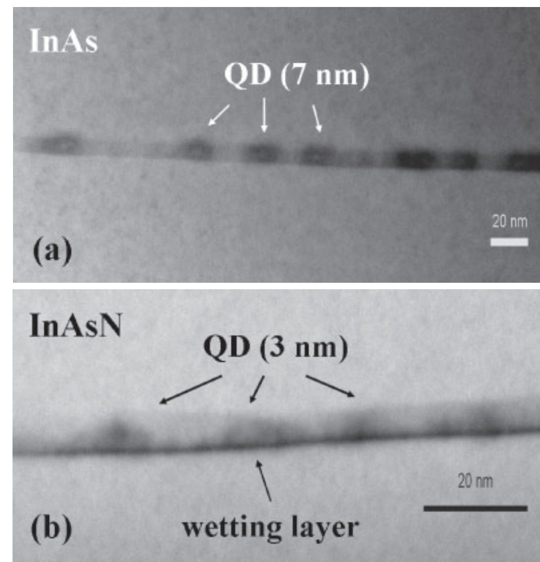

Fig. 7. Cross-sectional TEM images of (a) InAs QD sample and (b) InAsN QD sample.

be understood only as being caused by a change in the emission process by the E_{local} defect state. In fact, the InAsN QD sample emits at 1330 nm (at 300 K) with a low energy tail in the PL spectra, and similar low-energy tails were observed from N–As alloys which were attributed to the recombination of excitons that were trapped by localized states associated with the band tails[25] induced by inevitable composition fluctuation. Such a tail suggests composition fluctuation, which is inevitable at a high N content, and the presence of local regions with a N content higher than the average, which can be regarded as N clusters.[26]

4. Conclusions

The emission of electrons from N-induced localized defects in InAsN QDs is investigated. Two types of electron trap can be produced: one is associated with threading dislocations in the top GaAs layer and the other is associated with N-induced localized defects near the QDs. The threading dislocation energy at 648 meV can be explained by the crossing of the QD interface, where a band offset exists, by the trap. The incorporation of N into InAs QDs can introduce an additional capacitance plateau by generating an N-induced localized defect state, leading to additional carrier depletion at the bottom of the GaAs layer. This carrier depletion can suppress the electron tunneling emission from the InAs quantum state and change the electron emission process. Furthermore, the N-induced localized defects have finite density states, and the defect energy is confirmed to be from 0.3 to 0.36 eV below the quantum state (~0.2 eV), according to DLTS spectra. A simple C–V curve simulation is established which includes the QD state at 0.2 eV and N-induced localized defect at 0.36 eV below the GaAs conduction-band edge. A comparison of InAsN QDs with relaxed InAs QDs reveals composition fluctuation, which is inevitable at a high N content, and the presence of local regions that have a higher-than-average N content.

© 2011 The Japan Society of Applied Physics

Acknowledgments

The authors would like to thank Dr. R. S. Hsiao for preparing the samples and the National Science Council of the Republic of China, Taiwan, for financially supporting this research under Contract No. NSC-97-2112-M-009-014-MY3. This work was also supported by the ATU program of MOE.

1) M. Kondow, K. Uomi, A. Niwa, T. Kitatani, S. Watahiki, and Y. Yazawa: Jpn. J. Appl. Phys. **35** (1996) 1273.
2) F. Hohnsdorf, J. Koch, C. Agert, and W. Stolz: J. Cryst. Growth **195** (1998) 391.
3) S. Sato, Y. Osawa, T. Saitoh, and I. Fujimura: Electron. Lett. **33** (1997) 1386.
4) M. Kondow, S. Nakatsuka, T. Kitatani, Y. Yazawa, and M. Kai: Jpn. J. Appl. Phys. **35** (1996) 5711.
5) H. P. Xin and C. W. Tu: Appl. Phys. Lett. **72** (1998) 2442.
6) K. Nakahara, M. Kondow, T. Kitani, M. C. Larson, and K. Uomi: IEEE Photonics Technol. Lett. **10** (1998) 487.
7) S. R. Kurtz, A. A. Allerman, E. D. Jones, J. M. Gee, J. J. Banas, and B. E. Hammons: Appl. Phys. Lett. **80** (2002) 4777.
8) P. Krispin, S. G. Spruytte, J. S. Harris, and K. H. Ploog: Appl. Phys. Lett. **80** (2002) 2120.
9) M. A. Pinault and E. Tournie: Appl. Phys. Lett. **79** (2001) 3404.
10) H. P. Xin, K. L. Kavanagh, Z. Q. Zhu, and C. W. Tu: Appl. Phys. Lett. **74** (1999) 2337.
11) P. Krispin, S. G. Spruytte, J. S. Harris, and K. H. Ploog: J. Appl. Phys. **88** (2000) 4153.
12) R. J. Kaplar, S. A. Ringel, S. R. Kurtz, J. F. Klem, and A. A. Allerman: Appl. Phys. Lett. **80** (2002) 4777.
13) N. Holonyak, Jr., W. D. Laidig, B. A. Vojak, K. Hess, J. J. Coleman, P. D. Dapkus, and J. Bardeen: Phys. Rev. Lett. **45** (1980) 1703.
14) J. F. Chen, C. H. Yang, Y. H. Wu, L. Chang, and J. Y. Chi: J. Appl. Phys. **104** (2008) 103717.
15) T. Wosinski: J. Appl. Phys. **65** (1989) 1566.
16) Y. Uchida, H. Kakibayashi, and S. Goto: J. Appl. Phys. **74** (1993) 6720.
17) J. S. Wang, J. F. Chen, J. L. Huang, P. Y. Wang, and X. J. Guo: Appl. Phys. Lett. **77** (2000) 3027.
18) A. C. Irvine and D. W. Palmer: Phys. Rev. Lett. **68** (1992) 2168.
19) A. Hierro, J. M. Ulloa, J. M. Chauveau, A. Trampert, M. A. Pinault, E. Tournie, A. Guzman, J. L. Sanchez-Rojas, and E. Calleja: J. Appl. Phys. **94** (2003) 2319.
20) Y. D. Jang, J. S. Yim, U. H. Lee, D. Lee, J. W. Jang, K. H. Park, W. G. Jeong, J. H. Lee, and D. K. Oh: Physica E **17** (2003) 127.
21) J. F. Chen, R. S. Hsiao, P. C. Hsieh, Y. J. Chen, Y. P. Chen, J. S. Wang, and J. Y. Chi: J. Appl. Phys. **98** (2005) 113525.
22) C. M. A. Kapteyn, F. Heinrichsdorff, O. Stier, R. Heitz, and M. Grundmann: Physica E **13** (2002) 259.
23) S. Makino, T. Miyamoto, T. Kageyama, F. Koyama, and K. Iga: J. Cryst. Growth **221** (2000) 561.
24) J. F. Chen, R. S. Hsiao, Y. P. Chen, J. S. Wang, and J. Y. Chi: Appl. Phys. Lett. **87** (2005) 141911.
25) I. A. Buyanova, W. M. Chen, G. Pozina, J. P. Bergman, B. Monemar, H. P. Xin, and C. W. Tu: Appl. Phys. Lett. **75** (1999) 501.
26) J. F. Chen, R. S. Hsiao, P. C. Hsieh, J. S. Wang, and J. Y. Chi: J. Appl. Phys. **99** (2006) 123718.

© 2011 The Japan Society of Applied Physics